

Deribit 比特幣選擇權在隨機 波動度下的動態避險

Stochastic volatility dynamic hedging for Deribit BTC options

張詠淇^{*}

Yung-Chi Chang

鄧惠文^{**}

Huei-Wen Teng

沃夫岡·赫德勒^{***}

Wolfgang Karl Härdle

* 國立陽明交通大學應用數學系

Department of Applied Mathematics, National Yang Ming Chiao Tung University

** 通訊作者：國立陽明交通大學資訊管理與財務金融學系，新竹市東區大學路
1001 號；

Email: venteng@gmail.com

Department of Information Management and Finance, National Yang Ming Chiao Tung
University

*** 德國洪堡大學

Humboldt-Universität zu Berlin

投稿日期：2022 年 9 月 15 日；第一次修訂：2022 年 12 月 7 日；第二次修訂：2023 年
1 月 16 日；接受刊登日期：2023 年 1 月 19 日

Received : Sep. 15, 2022 ; First Revision : Dec. 7, 2022 ; Second Revision : Jan. 16, 2023 ;

Accepted : Jan. 19, 2023

作者感謝總編輯與兩位匿名評審委員惠賜寶貴意見與建議，讓本文論點更趨完善，所
有文責由作者自負。

Contents

- | | |
|--------------------------------------|--------------------------------|
| I. Introduction | III. Our methodology |
| II. Data | IV. Empirical analysis |
| 1. The Deribit BTC option | 1. Dynamic delta hedging |
| 2. Data descriptions | 2. Dynamic delta-gamma hedging |
| 3. Puzzles of the implied volatility | 3. Dynamic delta-vega hedging |
| 4. Model calibration | V. Conclusion |

摘 要

在近年加密貨幣選擇權市場中，Deribit 交易所提供了約 90% 的加密貨幣選擇權未平倉量。Deribit 中最大宗的選擇權類別是比特幣選擇權，是以比特幣 (BTC) 結算的合約因此允許專業交易員避免在加密貨幣以及法幣的頻繁轉換。然而，對於比特幣倒數型選擇權合理定價以及避險的研究仍舊需要精進。這一篇論文中，我們在 BS 模型和 Heston 隨機波動率模型下，針對 Deribit 比特幣選擇權的動態避險進行研究。在隨機波動率模型下，我們克服希臘字母在計算上的困難，提供新的希臘字母公式 (Delta, Gamma, Vega)。實證研究結果顯示，在考慮隨機波動率後，能有效增加在 Deribit 比特幣選擇權之定價與避險上的表現。

關鍵詞：Deribit 比特幣選擇權，隨機波動率模型，動態避險，希臘字母

Abstract

Deribit exchange offers about 90% open interest in the recent cryptocurrency options market. The dominating type of option listed in Deribit is the BTC option, which is settled in BTC and thus allows professional traders to avoid frequent convert between cryptocurrency and fiat currency. However, research on fair pricing and hedging for the inverse option still needs to be completed. In this paper, we conduct dynamic hedging of Deribit options under the BS model and the Heston stochastic volatility (SV) model. In addition, we provide novel formulae of Delta, Gamma, and Vega under the SV model. Our results show that adding the SV feature does enhance performances on pricing and hedging of Deribit options.

Keywords: Deribit BTC option, stochastic volatility model, dynamic hedging, Greeks

I. Introduction

Cryptocurrency is a digital currency based on Blockchain technology, which offers a unique way of securely recording and transferring information, such as a ledger of payments (Pagnottoni and Dimpfl, 2019). Since Satoshi (2008) coined the first cryptocurrency, Bitcoin (BTC) and the fast-increasing cryptocurrency (CC) market have surprised many investors. It took not long with the first BTC futures, which were listed in Chicago Board Options Exchange (CBOE) in December 2017 but soon discontinued. The Chicago Mercantile Exchange (CME) launched BTC futures in December 2017 as well, and a plethora of papers followed that focused on pricing and hedging this new asset class (Baur et al., 2018). Indeed, BTC futures allow institutional and retail investors to take positions betting on or hedging the price movement of BTC without actually staying in the crypto market. This brings us to the research question that we would like to present here: Pricing and hedging of CC-based products.

Deribit option exchange is the largest crypto option market at the time of writing down our thoughts. As shown in Table 1, about 90% of the open interest is on Deribit, followed by CME with only about 8% of the total. Moreover, Deribit only provides inverse contracts that have a position size in USD but are margined and settled in BTC. This kind of contract allows traders to trade using BTC without executing any transformation between it and any fiat currency on the same exchange. Therefore, one benefit is the reduction of transaction costs. However, there are limited studies on BTC-denominated Deribit BTC options.

The authors of Alexander et al. (2022) focus on the theoretical aspects of pricing crypto options using the Black-Scholes (BS) model, without delving into data analysis. In analyzing crypto options data, there are two main

approaches: (1) fitting a model to historical BTC returns and comparing the model and market options prices, and (2) fitting a model to Deribit options data. One example of the first approach is found in the work of Hou et al. (2020), who use a stochastic volatility model with correlated jumps (SVCJ) to model daily Bitcoin returns and simulate option prices for cryptocurrencies under this model. They provide sensitivity analysis based on simulated option prices but do not analyze actual option prices. Under a small open economy framework, Cao and Celik (2021) provide formulae for European options written on BTC, where BTC is treated as the equilibrium exchange rate. Model parameters are estimated from historical BTC prices, and option prices are calculated through analytic formulas based on model parameters estimated from historical BTC returns. Jalan et al. (2021) estimate the BS model and Heston-Nandi GARCH model with regimes switching in volatility from historical BTC returns. They compare model prices based on parameters estimated from historical BTC returns with Deribit options and find that the Heston-Nandi model predicts prices more accurately than the BS model.

Table 1: Total open interest on BTC derivative market

This table provides the open interest in each major exchange that sells BTC derivatives and was retrieved on July 12, 2022, from coinglass.com (<https://www.coinglass.com/options>)

Exchange	Open Interest (BTC)	%
Deribit	205.71K	88.3
CME	18.67K	8.0
Okex	7.10K	3.0
Bit.com	1.00K	0.4
LedgerX	500.53	0.2
FTX	1.61	0
Total	232.99K	100

The second approach to analyzing crypto options data is to calibrate model parameters using options data. Under the BS model, Zulfiqar and Gulzar (2021) study patterns of implied volatility based on short-dated (14-day maturity) Deribit options and show that BTC options belong to the commodity class of assets because of the presence of volatility forward skew in Bitcoin option data. In addition, Madan et al. (2019) compare the BS model, Laplace model, five variance gamma related models, and Heston stochastic volatility (SV) model, and calibrate model parameters by minimizing differences between model and market options prices. They find models with stochastic volatility provide a better fit. Recently, Teng and Härdle (2022) exploit Monte Carlo simulation with common random numbers to calibrate a stochastic volatility model with correlated jumps (SVCJ) models using BTC-denominated Deribit options. They implement dynamic delta hedging and found that the SVCJ model provides a better fit than nested models but is indistinguishable from the BS model in hedging errors.

One needs to calculate Greek formulae under a specific model to implement dynamic hedging. Greeks, such as deltas, gammas, and vegas, are mathematically partial differentiations of the option price with respect to parameters of interest. However, it is well-known that calculating higher-order Greeks, such as gammas, is numerically challenging (Glasserman, 2004). Broadie and Glasserman (1996) introduce two types of methods for calculating Greeks by identifying situations to swap the order of integration and differentiation. The likelihood ratio method (LRM) gives unbiased Greeks by differentiating the probability density of the underlying asset. However, LRM-based estimators are prone to have more significant variances. Variants of LRM include the measure-valued differentiation (Heidergott and Leahu, 2010; Thoma, 2012) and Malliavin calculus (Davis and Johansson, 2006; Kawai and Takeuchi, 2011). In contrast, the pathwise method differentiates the payoff function (Cao, 1985) and produces estimators of Greeks with lower variance. Because the pathwise method requires the payoff function

to satisfy Lipschitz continuity and additional regularity conditions, its application to higher-order Greeks is limited.

Motivated by the BS model, which is an established benchmark for pricing and hedging, we start with this rather simplistic geometric Brownian motion dynamics. Given the well-known non-constant implied volatility phenomena, financial econometric research and stochastic analysis have unfolded into several directions, among them jump models, local volatility models, and as a next layer also the SV model (Fengler, 2006). The SV model comprises the BS class but offers more calibration possibilities for the research done in this paper. In practice, one uses well-established numerical methods to fit SV models, see Heston (1993); Cui et al. (2017); Mrázek et al. (2016). We avoided GARCH or other time series-based techniques because they are not giving unique links to the stochastic volatility “world” (Franke et al., 2004).

This paper falls in the second category: We provide numerical feasibility to calibrate parameters of the Heston SV model using Deribit options so that we can investigate how parameters evolve over time in empirical analysis. In contrast to Teng and Härdle (2022), this paper focuses on the Heston stochastic volatility (SV) model and overcomes the difficulty in calculating high-order Greeks of the BTC-denominated Deribit BTC option under the SV model using the parameter derivative developed in Lyuu and Teng (2011) and Lyuu et al. (2019). We derive the higher-order Greeks formula (as a form of an expected value), and thus dynamic hedging strategies are explicitly implemented using Deribit options. We find that BS and SV models are indistinguishable in dynamic delta and delta-vega hedging, but the SV model outperforms the BS model in dynamic delta-gamma hedging. These Greeks allow us to implement subsequent dynamic hedging using actual Deribit options data. Compared with the BS model, we systematically examine whether the SV feature enhances the performance of hedging Deribit options.

This paper is organized as follows. Section II describes the data of the BTC-denominated Deribit BTC option and provides a review of the data. Section III presents formulas for the BTC-denominated Deribit BTC option's delta, gamma, and vega under the SV model. Section IV summarizes empirical analysis for dynamic hedging using real data of the BTC-denominated Deribit BTC option. The last section concludes. We defer the proofs to the Appendices.

II. Data

In this section, we first briefly contrast the USD- and BTC-denominated Deribit BTC options. Next, we move on to our data and discuss the given implied volatility. Then, we present the calibration procedure and price-fitting performance under the BS and SV models.

1. The Deribit BTC option

The Deribit BTC option tracks the USD value of a BTC but is settled in BTC. Deribit options can be quoted in both USD and BTC. Let ω denote the indicator for an option type: $\omega = 1$ for a call option and $\omega = -1$ for a put option. Let S_t be the average BTC index at time t (Madan et al., 2019). Given the time-to-maturity T of the contract, the payoff function for a USD-denominated BTC option (called a direct option for short) is

$$\wp^d(S_T) = \max\{\omega(S_T - K), 0\}, \quad (1)$$

and the payoff function for a BTC-denominated BTC option (called an inverse option for short) is

$$\wp^i(S_T) = S_T^{-1} \max\{\omega(S_T - K), 0\}. \quad (2)$$

Figure 1 contrasts the payoff plots of direct and inverse options in the upper and lower rows, respectively. It shows that the payoff of a inverse option possesses a curve feature. In addition, according to Eq. (2), the payoff of an inverse call is bounded by one BTC, and for an inverse put, the payoff can be huge for deep in-the-money contracts.

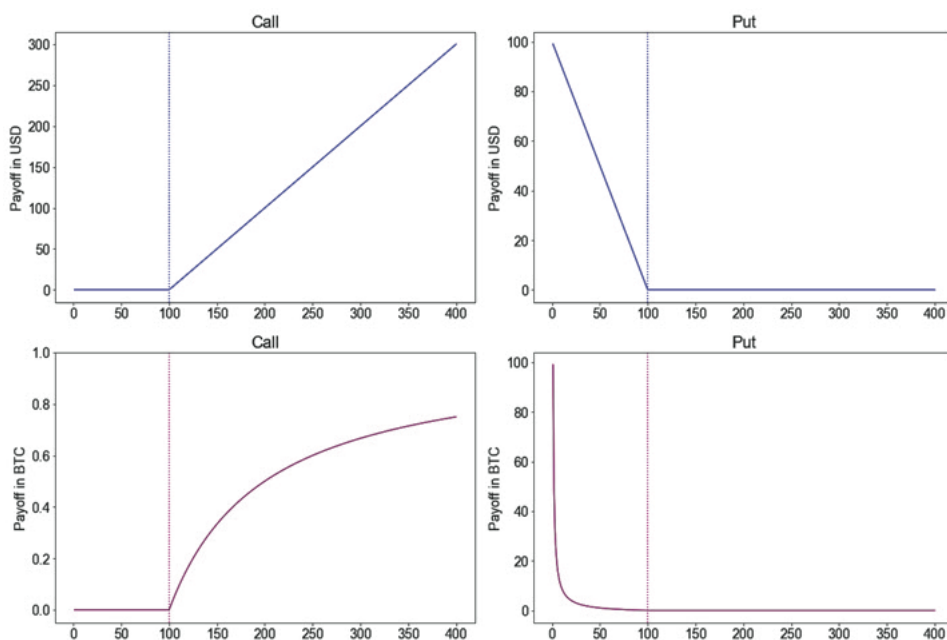


Figure 1: Payoffs of direct options and inverse options

This figure presents the payoff of the USD- and BTC-denominated call and put options against underlying prices in the upper and lower rows, respectively. Suppose $K = 100$.

 Deribit_inverse_BTC_options_hedging

2. Data descriptions

We retrieve the transaction data on inverse options in Deribit exchange from Blockchainresearch-center.com. The whole time frame is from April 14,

2021, to February 15, 2022. Table 2 shows the average daily proportion of contracts in each moneyness-maturity category. It shows that, on average, about 75% of traded contracts expire in 30 days or less, and about 70% of them are classified as out-the-money options. Most call and put options are traded short-term and out-of-the-money. Similar observations can be seen in Figure 2, which provides the scatter plot of transactions on September 21, 2021.

Figure 3 displays the BTC prices from April 14, 2021, to February 15, 2022. The prices range from about 30,000 to 70,000 during the whole period, which indicates they are pretty volatile. Figure 4 provides the scatter of the semi-log plots for the transactions of inverse options during the period, where the left and right panels are for call and put options, respectively. These plots indicate the wide range of strikes in both call and put options from about 20,000 to 400,000. In addition, Figure 4 shows that the range of strike prices of an inverse option is mainly between the current index price and 10,000 greater and that the range of strike prices of an inverse put option is mainly between the current index price and 5,000 less.

Table 2: Average daily proportion of inverse contracts

The table provides the average daily proportion of inverse contracts in each moneyness-maturity category. The call options are divided as OTM, ATM, and ITM if the moneyness $K/S_t \geq 1.025$, $0.975 < K/S_t < 1.025$, and $K/S_t \leq 0.975$, respectively. The put options are divided as OTM, ATM, and ITM if the moneyness $K/S_t \leq 0.975$, $0.975 < K/S_t < 1.025$, and $K/S_t \geq 1.025$, respectively.

Class	Call			Put			Total
	OTM	ATM	ITM	OTM	ATM	ITM	
$0 \leq T \leq 30$	25.65	12.56	1.66	22.26	11.37	1.83	75.34
$31 \leq T \leq 60$	5.43	0.46	0.33	3.61	0.49	0.43	10.76
$T \geq 61$	7.98	0.26	0.40	4.22	0.33	0.72	13.91
Total	39.07	13.27	2.40	30.09	12.20	2.98	100.00

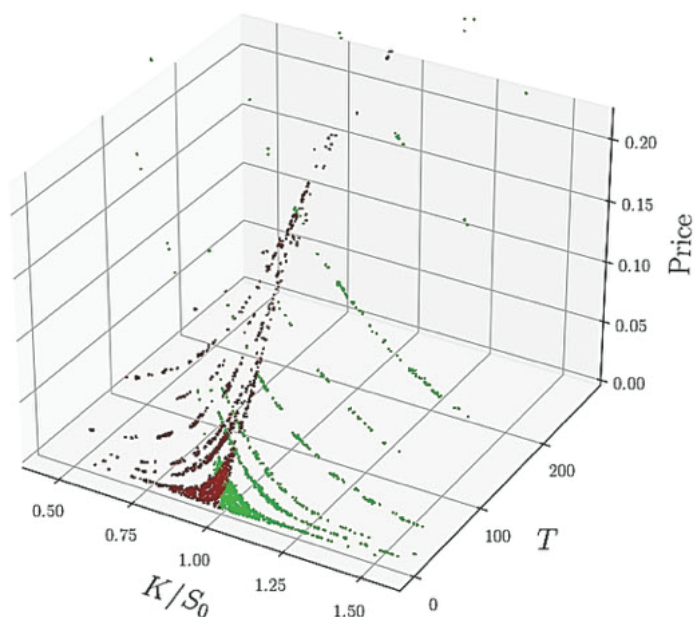


Figure 2: Scatter plot of Deribit inverse options traded on September 21, 2021

The green dots represent the call option, and the red dots represent the put option.

Deribit_inverse_BTC_options_hedging

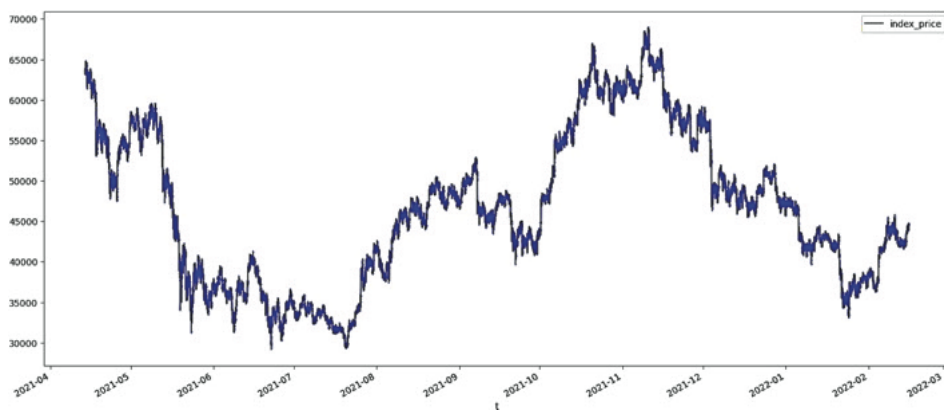


Figure 3: Time series of BTC perpetual futures index price

The timeframe is from April 14, 2021, to February 15, 2022. Deribit_inverse_BTC_options_hedging

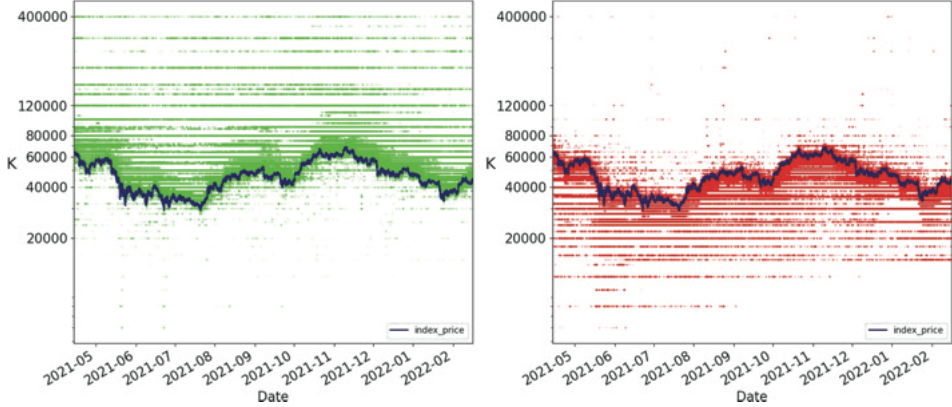


Figure 4: Scatter of semi-log plots of Deribit inverse options traded

The left and right panels indicate the call options (green) and the put options (red).

 Deribit_inverse_BTC_options_hedging

3. Puzzles of the implied volatility

Let r and q denote the interest rate and the dividend yield, respectively. Let $\Phi(\cdot)$ denote the cumulative distribution function of the standard normal distribution, respectively. The implied volatility provided by Deribit is denoted by iv . To check if Deribit uses the payoff function of an inverse option, we examine iv as follows. First, let $m_{BS}^d \stackrel{\text{def}}{=} m_{BS}^d(\sigma; \omega, T, K)$ and $m_{BS}^i \stackrel{\text{def}}{=} m_{BS}^i(\sigma; \omega, T, K)$ denote the pricing formula of the direct option and inverse option under the BS model, respectively. We employ the BS formulas for the direct and inverse options in Alexander and Imeraj (2021), respectively:

$$m_{BS}^d = \omega \left\{ e^{-qT} S_0 \Phi(\omega d_1) - e^{-rT} K \Phi(\omega d_2) \right\}, \quad (3)$$

$$m_{BS}^i = \omega \left\{ e^{-rT} \Phi(\omega d_2) - e^{(q-r+\sigma^2)T} S_0^{-1} K \Phi(\omega d_3) \right\}, \quad (4)$$

Where

$$d_1 = \frac{\log\left(\frac{S_0}{K}\right) + (r - q + \frac{1}{2}\sigma^2)T}{\sigma\sqrt{T}}, \quad d_2 = d_1 - \sigma\sqrt{T}, \quad d_3 = d_2 - \sigma\sqrt{T}.$$

Similar to Hou et al. (2020) and Matic et al. (2021), we set $r = 0$ and $q = 0$ because the interest rate is very close to zero during our study period and there is no dividend paid in investing BTC. Now, we calculate σ_{BS}^d and σ_{BS}^i , so that they match the theoretical price for the direct and inverse option in Eqs. (3) and (4), respectively. In other words, σ_{BS}^d and σ_{BS}^i satisfy

$$m_{BS}^i(\sigma_{BS}^i; \omega, T, K) = p(\omega, T, K),$$

$$m_{BS}^d(\sigma_{BS}^d; \omega, T, K) = p(\omega, T, K),$$

where $p(\omega, T, K)$ is the market price of an option with type ω , time to maturity T , and strike K .

Using 3-dimensional scatter plots, Figure 5 compares iv , σ_{BS}^d and σ_{BS}^i against strike price and time-to-maturity with intraday transactions of inverse options on September 30, 2021. Note that iv and σ_{BS}^d scatter similarly, but σ_{BS}^i has visibly different patterns: σ_{BS}^i has higher curvature given a time-to-maturity τ . This pattern also appears on other trading days. Thus, it is likely that Deribit uses the payoff of a direct option to extract iv .

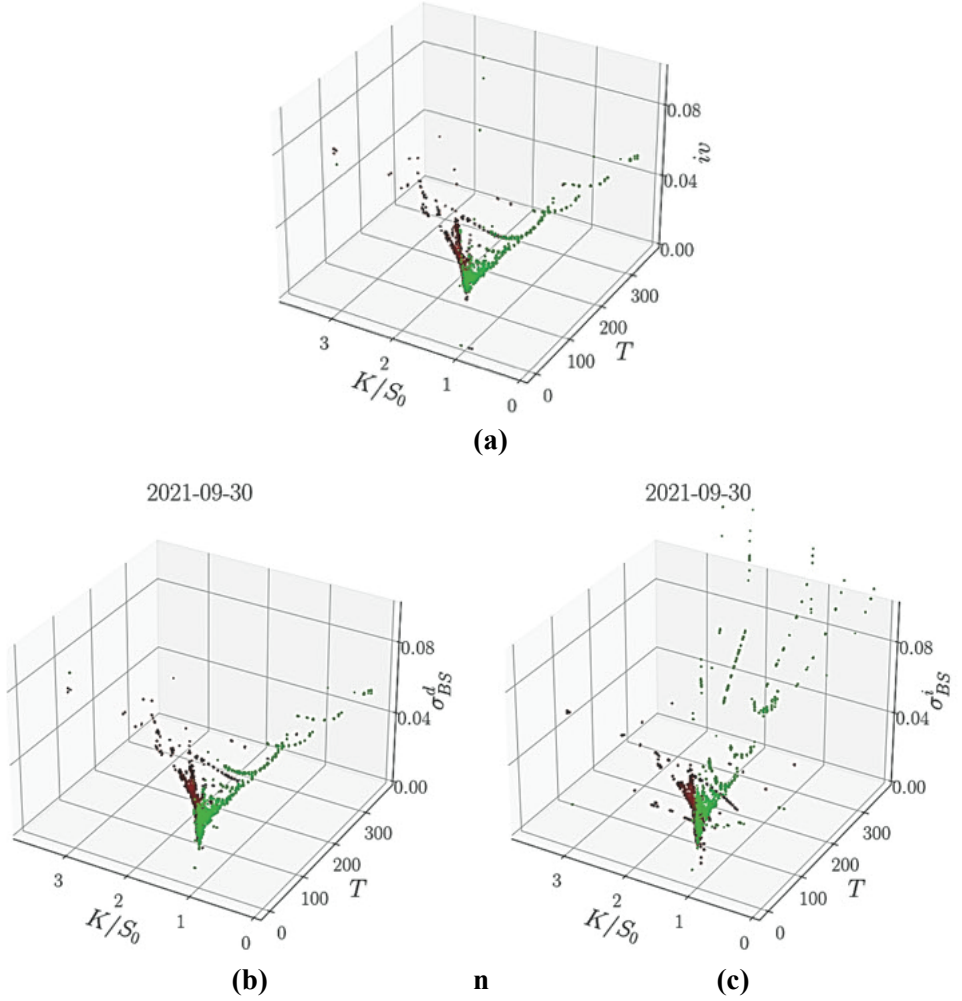


Figure 5: Implied volatility iv , σ_{BS}^d and σ_{BS}^i

The upper, middle, and lower panels provide 3-dimensional scatter plots for three types of implied volatility against moneyness and time to maturity: iv from Deribit, σ_{BS}^d extracted from the BS formula for a direct option, and σ_{BS}^i extracted from the BS formula for an inverse option, respectively. The green and red dots indicate call and put options, respectively. Here, we use intraday transactions of Deribit inverse options on September 30, 2021.

Next, we plug iv to Eqs. (3) and (4), respectively, to check if they produce option prices that match the market prices $p(\omega, T, K)$. When using the payoff of a direct option, we multiply the option price by the market price of a BTC in USD, so that the option price is denominated in USD. Figure 6 provides a scatter plot of market prices for the option in BTC against model prices of the inverse option using iv in the left panel, and market prices for the option in USD against model prices of the direct option using iv in the right panel, respectively. It is shown that, in the right panel, more points lay on the 45-degree straight line. This suggests again that the Deribit is likely to use the payoff function of a direct option to calculate the implied volatility.

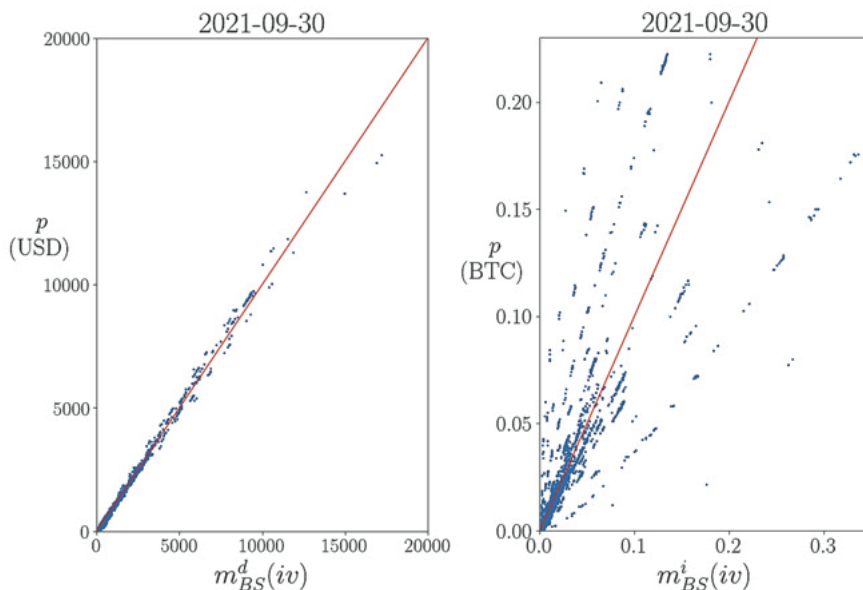


Figure 6: Pricing inverse options with BS formulae through iv

The left and right panels provide scatter plots of the market price for an inverse option p versus the model price using the BS formula for a direct option $m_{BS}^d(iv)$ and the BS formula for an inverse option $m_{BS}^i(iv)$ respectively. We overlay a 45-degree straight line in each panel and use intraday transactions of Deribit inverse options on September 30, 2021.

In Figure 7, we compare scatter plots of iv versus σ_{BS}^d in the left panel and iv versus σ_{BS}^i in the right panel, respectively. Interestingly, points deviate from the 45-degree straight line in both panels, and this indicates that the iv provided by Deribit differs from our calculated σ_{BS}^d and σ_{BS}^i . However, points in the left panel are more clustered to the 45-degree straight line. Thus, it is likely that Deribit uses the payoff function of a direct option to exact the implied volatility.

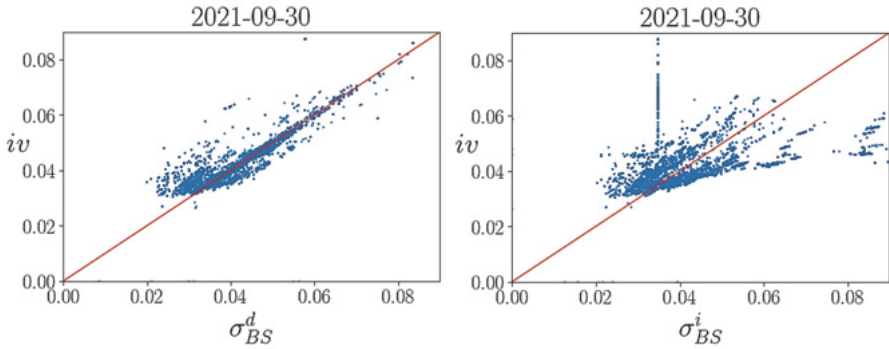


Figure 7: Discrepancies between iv and σ_{BS} 's

The left and right panels provide scatter plots of iv versus σ_{BS}^i and iv versus σ_{BS}^d , respectively. We overlay a 45-degree straight line in each panel and use intraday transactions of Deribit inverse options on September 30, 2021.

4. Model calibration

To calibrate a model and obtain implied parameters, so that model prices are consistent with market prices, we follow Bakshi et al. (1997) to minimize a loss function defined as

$$\mathcal{L}(\Theta) = \sum_{i=1}^N \{ \mathcal{C}_{\Theta}(\omega_i, K_i, T_i) - \mathcal{C}(\omega_i, K_i, T_i) \}^2, \quad (5)$$

where Θ is the set of parameters of the option pricing model, N is the number of contracts available. For the i -th contract, ω_i is the option type, K_i is the strike

price, and T_i is the time-to-maturity. In addition, $C_\Theta(\cdot)$ is the theoretical option price, and $C(\cdot)$ is the market option price. The estimated parameter is denoted as $\hat{\Theta}$, which is the minimizer of the loss function (5):

$$\hat{\Theta} = \arg \min_{\Theta} \mathcal{L}(\Theta).$$

Let W_t be a Wiener process. Under the risk-neutral measure, the dynamics of the underlying asset in the BS model follows

$$\frac{dS_t}{S_t} = r dt + \sigma dW_t.$$

Instead of assuming constant variance, the Heston stochastic volatility (SV) model assumes that the variance of the underlying asset return follows the mean-reverting CoxIngersoll-Ross (CIR) process. Under the risk-neutral measure, the dynamics of the underlying asset in the SV model follows

$$\begin{aligned} \frac{dS_t}{S_t} &= r dt + \sqrt{V_t} dW_t^S \\ dV_t &= \kappa(\theta - V_t) dt + \sigma_v \sqrt{V_t} dW_t^V \\ \text{Cov}(dW_t^S, dW_t^V) &= \rho dt \end{aligned}$$

where κ is the speed of mean reversion in a volatility process, θ is the long-term mean of the volatility process, σ_v is the volatility in the volatility, and ρ is the correlation of two Wiener processes.

To price the inverse option, we use the Euler-Maruyama simulation scheme to generate the underlying price and use the sample mean of the payoff function to estimate the price of an option. On a daily basis, we simulate the stock price $S(t)$ and volatility $V(t)$ at time t for $t = 1, \dots, T$. We also abbreviate $S(0) = S_0$ and

$S(T) = S_T$ for convenience. The discretization scheme is presented as follows:

$$\log S(t) - \log S(t-1) = \left(r - \frac{V(t)}{2} \right) + \sqrt{V(t)} X(t) \quad (6)$$

$$V(t) = \alpha + \beta V(t-1) + \sigma_v \sqrt{V(t-1)} Y(t) \quad (7)$$

where $\alpha = \kappa\theta$, $\beta = 1 - \kappa$. And, X_t and Y_t are constructed by

$$\begin{bmatrix} Y(t) \\ X(t) \end{bmatrix} = \begin{bmatrix} 1 & 0 \\ \rho & \sqrt{1-\rho^2} \end{bmatrix} \times \begin{bmatrix} Z_{Y,t} \\ Z_{X,t} \end{bmatrix}, \quad (8)$$

where $Z_{Y,t}$ and $Z_{X,t}$ are independent standard normal random variables. Further, since the volatility process should be strictly positive, Feller's condition is required. That is,

$$2\kappa\theta > \sigma_v^2 \quad \Leftrightarrow \quad 2\alpha > \sigma_v^2 \quad (9)$$

For the SV model, the option price is calculated as the mean payoff based on multiple simulated paths through the Monte Carlo simulation. Details using common random numbers in reducing variation in Monte Carlo simulation can be found in Teng and Härdle (2022). In the SV model, we need to estimate five parameters:

$$\Theta = \{\rho, \alpha, \beta, V_0, \sigma_v\}.$$

The calibration process is implemented daily from April 14, 2021, to January 31, 2022. We use all the traded contracts available on the given date as inputs, and the estimated parameters $\hat{\Theta}$ are obtained daily by minimizing the

loss function in Eq. (5). Figure 8 shows the time series plots for each implied parameter in which the BS parameters are colored in black, and the SV parameters are colored in blue. The figure shows that ρ and V_0 in the SV model have peaks that significantly deviate from their medians, and the time series for β fluctuations is quite volatile during the period. This volatility might refer to the numerical difficulties in calibrating the models with stochastic volatility, where different sets of parameters give the same value in terms of the loss function.

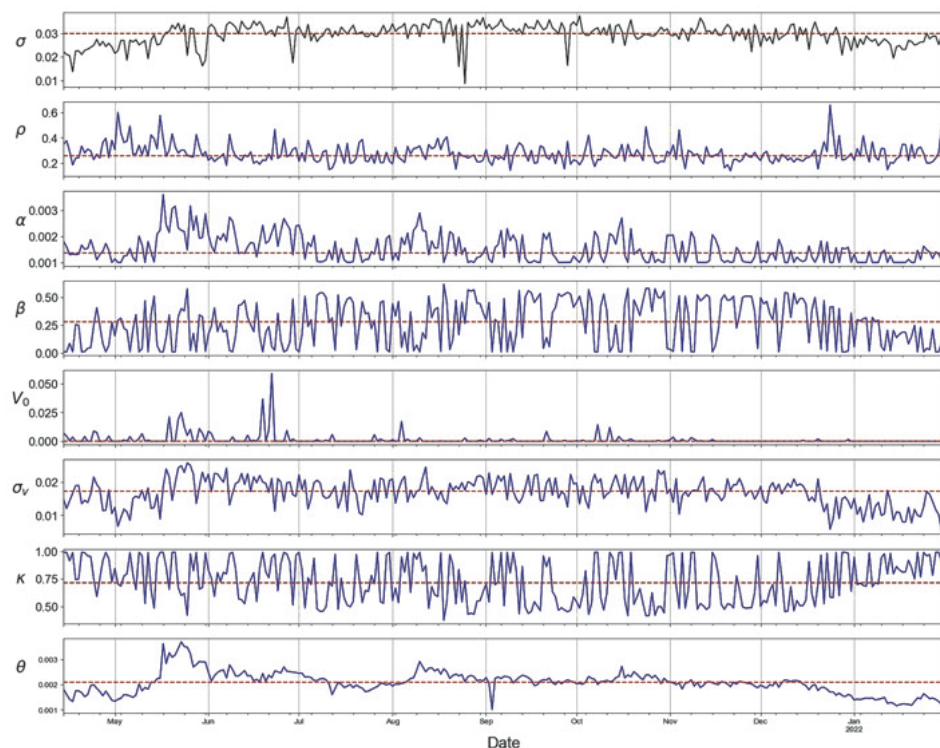


Figure 8: Time series of implied parameters

The black lines are the implied parameters under the BS model, and the blue lines are those under the SV model. The red dashed lines represent the medians for each time series.

Deribit_inverse_BTC_options_hedging

We compare the RMSE, MAE, and MAPE for a robustness check to identify their sample pricing error. These metrics are calculated as follows:

$$\begin{aligned}
 RMSE(\Theta) &= \sqrt{\frac{1}{N} \sum_{i=1}^N \left(\mathcal{C}_{\Theta}(\omega_i, K_i, T_i) - \mathcal{C}(\omega_i, K_i, T_i) \right)^2} \\
 MAE(\Theta) &= \frac{1}{N} \sum_{i=1}^N \left| \mathcal{C}_{\Theta}(\omega_i, K_i, T_i) - \mathcal{C}(\omega_i, K_i, T_i) \right| \\
 MAPE(\Theta) &= \frac{1}{N} \sum_{i=1}^N \frac{|\mathcal{C}_{\Theta}(\omega_i, K_i, T_i) - \mathcal{C}(\omega_i, K_i, T_i)|}{\mathcal{C}(\omega_i, K_i, T_i)}
 \end{aligned}$$

Figure 9 presents the time series plots of RMSE, MAE, and MAPE for each date for the BS and SV models. For RMSE and MAE, the SV model produces more minor errors with smaller variances, similar to the MAE case. For the MAPE, it shows that the SV model yields more minor errors most of the time but with more significant variances, especially starting from August 2021. This result is as expected since more parameters are involved in the SV model, which can represent more complicated dynamics for the stock price process.

For in-sample analysis, we calibrate the model parameters on day t using intraday option prices and calculate the in-sample RMSE, MAE, and MAPE. We calculate the out-of-sample RMSE, MAE, and MAPE, between the market price on the day $(t + 1)$ and the model price on the day $(t + 1)$ with implied parameters calibrated on the day t . Therefore, the out-of-sample period is from April 15, 2021, to January 31, 2022. Figure 10 provides the time series of the out-of-sample pricing error for each metric for the BS and SV models. It shows that all the metrics have smaller values in the SV model, despite the significant variance in terms of MAPE. These values indicate that there is no over-fitting phenomenon in the SV model.

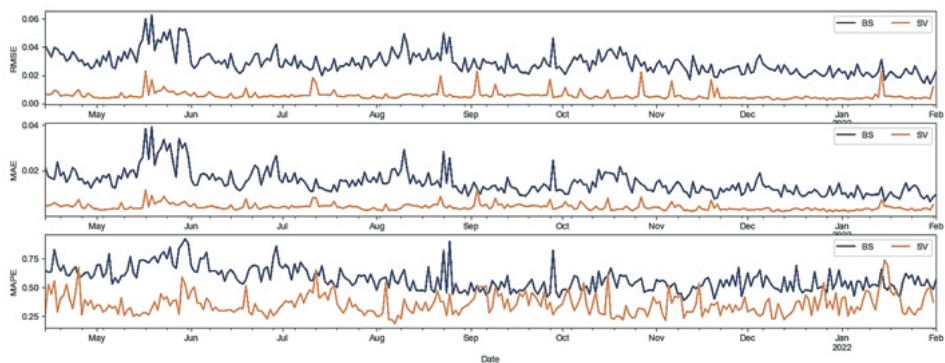


Figure 9: Time series plots of in-sample pricing error

The upper, middle, and bottom panels provide time series plots for RMSE, MAE, and MAPE under the BS and SV models, respectively.

Deribit_inverse_BTC_options_hedging

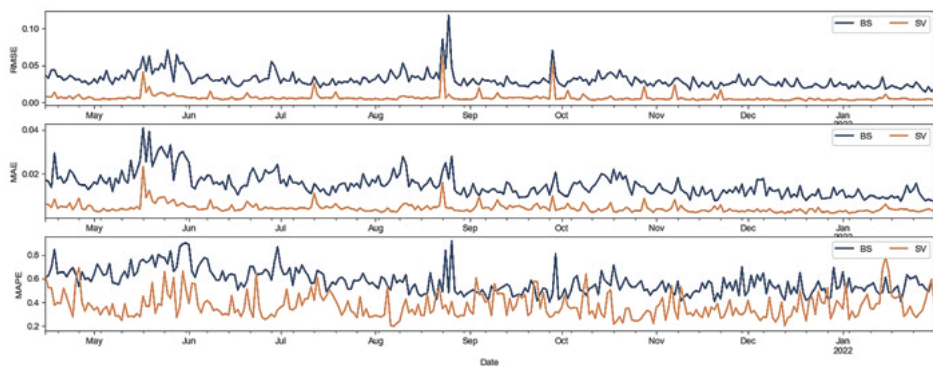


Figure 10: Time series plots of out-of-sample pricing error

The upper, middle, and bottom panels provide time series plots for RMSE, MAE, and MAPE under the BS and SV models, respectively.

Deribit_inverse_BTC_options_hedging

III. Our methodology

To start, we set $r = q = 0$ throughout this paper because the interest rate is close to zero during the study period. Let $I_{\{\cdot\}}$ denote the indicator function. Alexander and Imeraj (2021) provide the delta (Δ_{BS}), gamma (Γ_{BS}), and vega (\mathcal{V}_{BS}) for the BS model:

$$\Delta_{BS} = \omega e^{\sigma^2 T} S_0^{-2} K \Phi(\omega d_3), \quad (10)$$

$$\Gamma_{BS} = e^{\sigma^2 T} S_0^{-3} K \left\{ \phi(\omega d_3) (\sigma \sqrt{T})^{-1} - 2\omega \Phi(\omega d_3) \right\}, \quad (11)$$

$$\mathcal{V}_{BS} = \phi(d_2) \sqrt{T} - 2\omega e^{\sigma^2 T} \sigma T S_0^{-1} K \Phi(\omega d_3). \quad (12)$$

To address the challenge of calculating Greeks under the SV model, we adopt the methods outlined in Lyuu et al. (2019) to derive the following formulas. To begin, we remind the reader of the concept of the parameter derivative. Suppose the underlying asset S can be considered as a function whose input is made up of a parameter of interest θ and a random vector $X = (X_1, X_2, \dots, X_m)^\top \in \mathbb{R}^m$ under suitable simulation scheme. For a financial derivative that has discounted payoff function related to the underlying S , denoted by $\wp(\theta, X)$, its price is equal to

$$c(\theta) = \mathbb{E}[\wp(\theta, X)] = \int_{\mathbb{R}^m} \wp(\theta, x) f(x) dx$$

where $x = (x_1, x_2, \dots, x_m)^\top$ represents a realization of X . The parameter derivative is defined as follows:

Definition 1 Suppose the price function $c(\theta)$ is differentiable with respect to θ . The **parameter derivative of $\wp(\theta, x)$ with respect to θ** is a function $D_{\theta}\wp(\theta, x)$ on \mathbb{R}^m satisfying

$$\int_{\mathbb{R}^m} D_{\theta}\wp(\theta, x) f(x) dx = \frac{\partial}{\partial \theta} \int_{\mathbb{R}^m} \wp(\theta, x) f(x) dx$$

Our approach is to calculate the parameter derivative of the payoff function \wp , which would then allow us to estimate the Greek sensitivity measures through Monte Carlo simulation. To save space, the reader can refer to Chang (2022) for a numerical examination of the accuracy and efficiency of the proposed Greeks estimators in the following context. First, Theorem 1 gives the delta formula.

Theorem 1 The delta of the inverse option under the SV model is

$$\Delta = \mathbb{E} \left[\omega \left(\frac{1}{S_0} \frac{K}{S_T} \right) I_{\{\omega(S_T - K) > 0\}} \right]. \quad (13)$$

Proof. Please see Appendix 1.

As displayed in Figure 11, the delta of call and put options under the BS and SV models show similar values for short-term contracts, but the differences between the models become more pronounced as the time-to-maturity increases. Furthermore, the trend of the deltas is consistent between the two models, however, the values of deltas are small, typically around 10^{-5} . Additionally, the overall patterns in the SV model are flatter across various levels of moneyness, which aligns with the more volatile dynamics of the underlying asset price in the SV model.

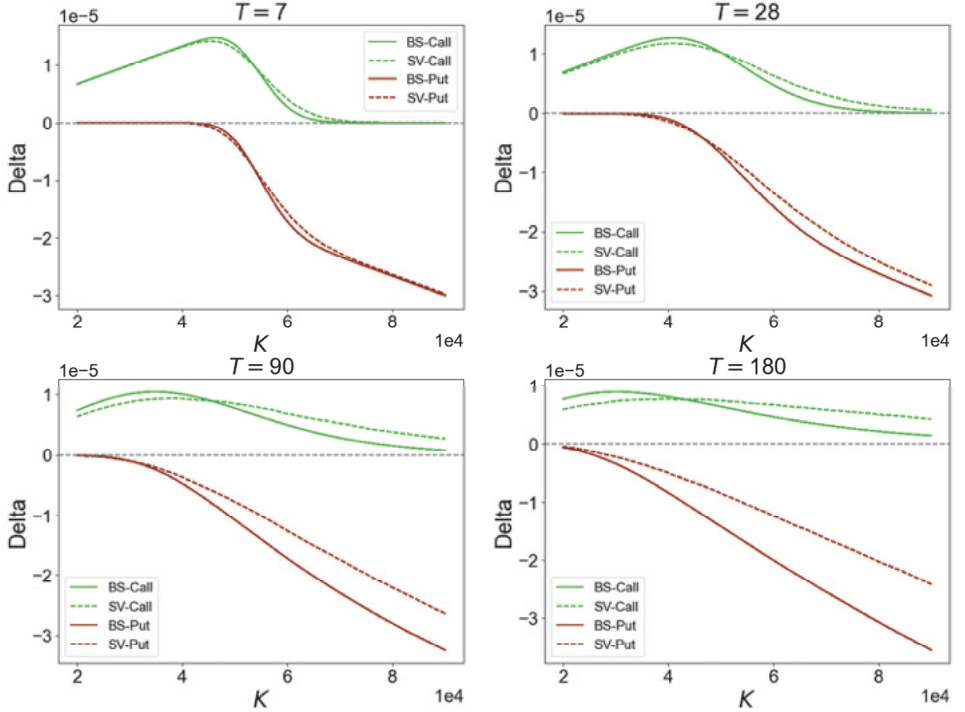



Figure 11: Delta comparison among different time-to-maturities

The following figure shows the case when $S_0 = 55,000$ by using the implied parameters induced by the contracts available on September 30, 2021. ($\sigma_{BS} = -0.0548$, $\rho = 0.2252$, $\alpha = 0.0012$, $\beta = 0.4119$, $V_0 = 0.0001$, and $\sigma_v = 0.0194$)  Deribit_inverse_BTC_options_hedging

Second, Theorem 2 gives the gamma formula.

Theorem 2 *The gamma of the inverse option under the SV model is*

$$\Gamma = \mathbb{E} \left[\omega \left(\frac{-2 K}{S_0^2 S_T} \right) I_{\{\omega(S_T - K) > 0\}} \right] - \mathbb{E}^* \left[\frac{1}{S_0} f_{Z_{X,T}}(\chi) \frac{\partial \chi(S_0, V_0, Z_{X,-T}, Z_Y)}{\partial S_0} \right]$$

where $Z_{X,-T} \sim \mathcal{N}(0, \mathbb{I}_{T-1})$, $Z_Y \sim \mathcal{N}(0, \mathbb{I}_T)$ under $\mathbb{E}^*[\cdot]$,

$$\chi = \frac{1}{\sqrt{1-\rho^2}} \left[\frac{\log \left(\frac{K}{S_0 h(Z_{X,-T}, Z_Y)} \right) - \left(r - \frac{V_T}{2} \right)}{\sqrt{V_T}} - \rho Z_{Y,T} \right]$$

$$\frac{\partial \chi(S_0, V_0, Z_{X,-T}, Z_Y)}{\partial S_0} = \frac{-1}{\sqrt{(1-\rho^2)V_T S_0}},$$

$$h(Z_{X,-T}, Z_Y) = \prod_{t=1}^{T-1} e^{\gamma_t}$$

Proof. Please see Appendix 2.

Figure 12 illustrates the gammas of call and put options under the BS and SV models. The gammas of call contracts are either positive or negative, while those of put contracts are always positive regardless of the time-to-maturity. Furthermore, the pattern of the gammas is consistent between the two models and their values are small, typically around 10^{-9} . Additionally, the overall patterns in the SV model are less pronounced across different levels of moneyness, which is consistent with the more volatile dynamics of the underlying asset price in the SV model.

As for the SV model, we refer to Zhu (2009) that the long-term mean of the variance θ is not related to the adjustment of the hedging portfolio at the rebalance date. Here, we only consider the spot volatility V_0 for calculating vega under the SV model. In other words, we consider vega as the partial differentiation of the option price with respect to the $\sqrt{V_0}$ under the SV model and use it for the whole dynamic hedge process. This use coincides with the definition of vega under the BS model. We provide the Vega formulain Theorem 3.

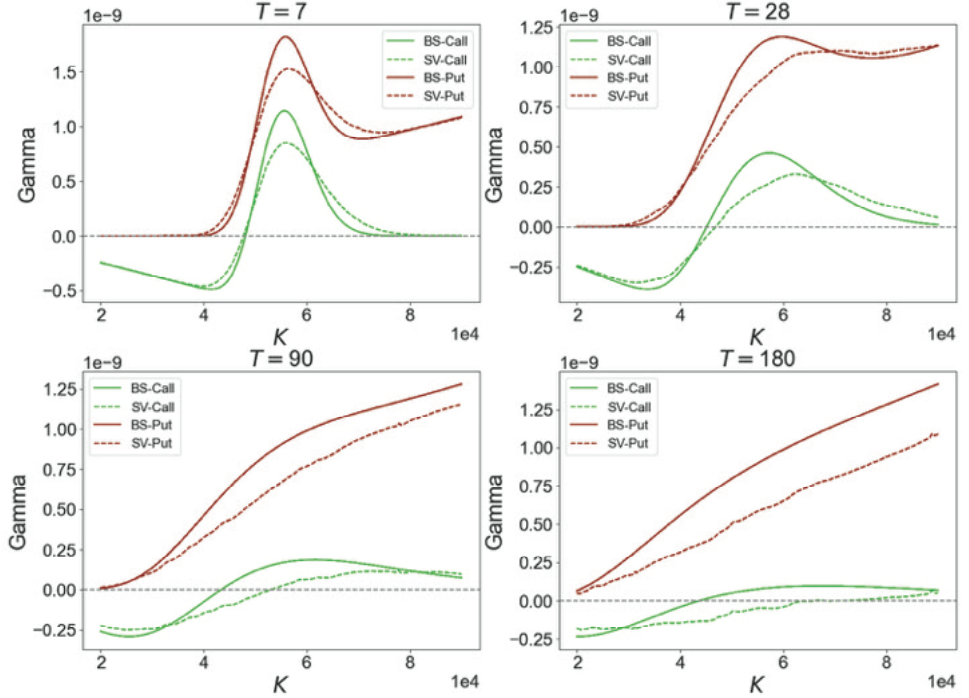


Figure 12: Gamma comparison among different time-to-maturities

The following figure shows that when $S_0 = 55,000$, the implied parameters induced by the contracts available on September 30, 2021, are $\sigma_{BS} = 0.0348$, $\rho = 0.2252$, $\alpha = 0.0012$, $\beta = 0.4119$, $V_0 = 0.0001$, and $\sigma_v = 0.0194$. [Deribit_inverse_BTC_options_hedging](#)

Theorem 3 *The vega of the inverse option under the SV model is*

$$\mathcal{V} = \mathbb{E} \left[\omega \left(\frac{K}{S_T} \sqrt{V_0} \sum_{j=1}^T \left[\left(-1 + \frac{X_j}{\sqrt{V_j}} \right) \left(\prod_{t=1}^j G(V_{t-1}, Y_t) \right) \right] \right) I_{\{\omega(S_T - K) > 0\}} \right]$$

where

$$G(V_{t-1}, Y_t) = \beta + \frac{\sigma_v Y_t}{2\sqrt{V_{t-1}}}$$

Proof. Please see Appendix 3.

Figure 13 shows the vega for call and put options under the two different models. It shows that the patterns of vegas are quite contrasting. It is important to note that the definition of vega is different between the two models. The figure shows that the vega of call options is more significant than that of put options in the SV model, while it is the opposite in the BS model. Additionally, the magnitude of vega is substantial, with values around 10^{-2} or 10^{-3} , which is more significant compared to delta and gamma.

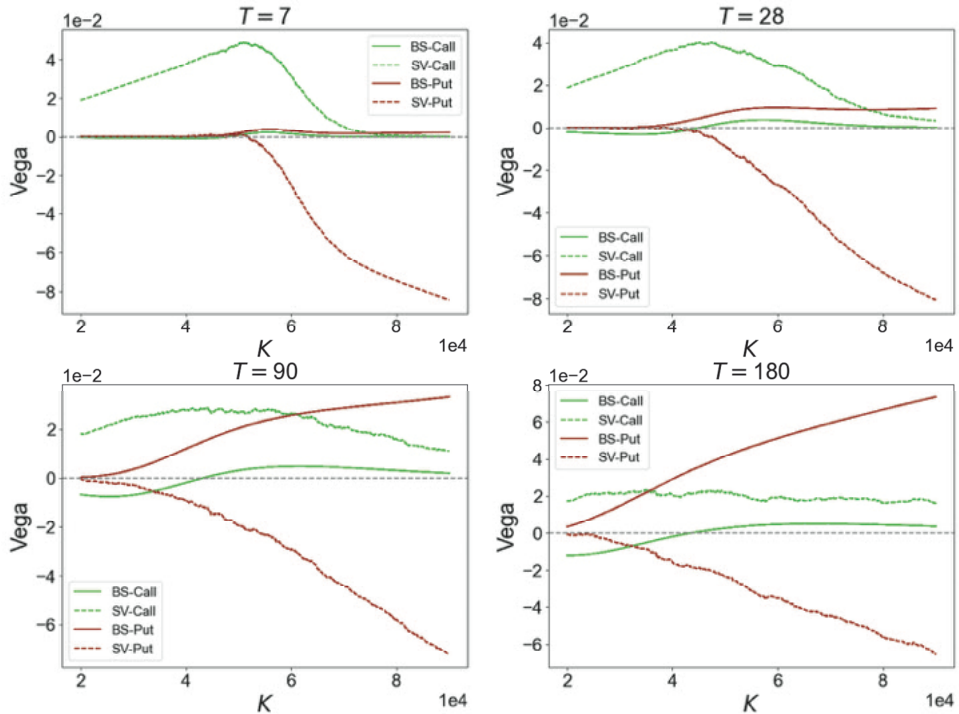


Figure 13: Vega comparison among different time-to-maturities

The following figure shows that when $S_0 = 55,000$, the implied parameters are induced by the contracts available on September 30, 2021. ($\sigma_{BS} = 0.0348$, $\rho = 0.2252$, $\alpha = 0.0012$, $\beta = 0.4119$, $V_0 = 0.0001$, and $\sigma_v = 0.0194$) [Deribit_inverse_BTC_options_hedging](#)

IV. Empirical analysis

This section comprises three dynamic hedging routines, and we summarize the empirical dynamic hedging performances.

1. Dynamic delta hedging

Suppose we hedge in discrete time t for which $t = 0, 1, 2, \dots, T$, where T is the time-to-maturity of a given option contract. Let $P(t)$, $S(t)$ be the option price and the underlying index price at time t ; and let $\Delta(t)$, $\Gamma(t)$, $\mathcal{V}(t)$ be the delta, gamma, and vega of an option at time t , respectively. Consider the delta-neutral portfolio:

1. A short position of an inverse option, $-P(t)$, denominated in BTC.
2. Long $\Delta(t)$ BTCs.
3. A position in the money market, $B(t)$, denominated in USD.

Let $\Pi(t)$ denote the value of this portfolio denominated in USD. At first, set

$$B(0) = P(0)\overline{S(0)} - \Delta(0)S(0).$$

Then, we have

$$\Pi(0) = -P(0)\overline{S(0)} + \Delta(0)S(0) + B(0) = 0.$$

Here, we use $\overline{S(0)}$ to denote that it is a constant to consistently denote the option price in USD that will not be affected by changes in $S(t)$. For each time with $t \neq T$ we adjust the position of BTC from $\Delta(t-1)$ to $\Delta(t)$ and add value changes in BTC to the money market account:

$$B(t) = e^{r(t-t-1)}B(t-1) - S(t)[\Delta(t) - \Delta(t-1)].$$

As a result, we have the following:

$$\Pi(t) = -P(t)S(t) + \Delta(t)S(t) + B(t).$$

We get the hedging portfolio value $\Pi(T)$ by repeating the above procedure until maturity. To measure the performance of hedging, we determine the discounted relative hedging error,

$$\pi = \frac{e^{-rT}\Pi(T)}{P(0)\bar{S}(0)}.$$

The contracts we use for the out-of-sample analysis are those with time-to-maturities ranging from 2 to 28 days and issued from April 14 to December 31, 2021. We only use the latest transaction for options with the same type, time-to-maturity, and strikes issued on exact dates. Throughout this paper, the hedge is rebalanced daily. The delta is calculated using parameters implied on the previous date. To have more contracts for hedging, we hedge each option until one day before maturity. The above setting applies to the dynamic delta-gamma and delta-vega hedging.

To present the results, we divide the contracts into three groups based on their time-to-maturity: $2 \leq T \leq 7$, $8 \leq T \leq 14$, and $15 \leq T \leq 28$. Figures 14 and 15 show the hedging performance on inverse call and put options using the dynamic delta hedge for each moneyness-maturity category. First, for call options, Figures 14 show no difference between the two models for each type. All box plots have an upper bound of one and are not centered at zero. Figure 15 shows a similar phenomenon for put options. Next, for OTM and ITM contracts, the box plots of the relative hedging error become narrower as we consider longer time-to-maturity contracts.

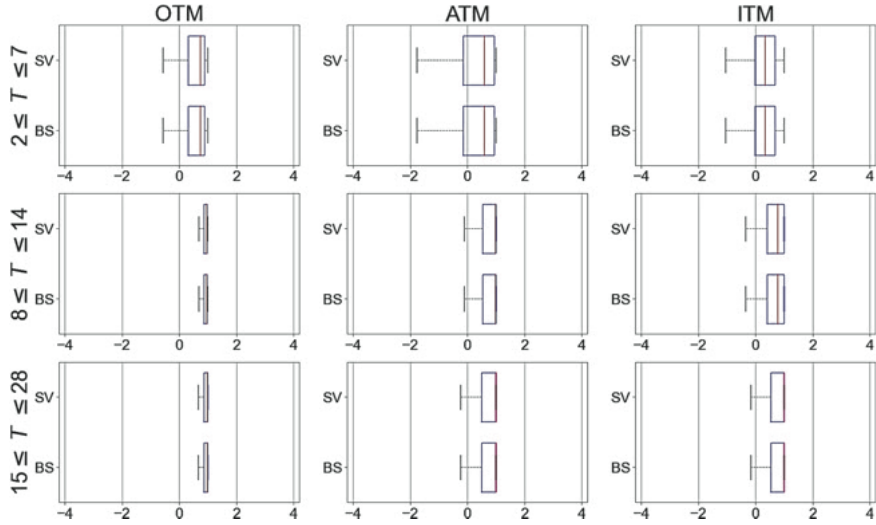


Figure 14: Relative hedging errors for inverse call options using the dynamic delta hedge ■ Deribit_inverse_BTC_options_hedging

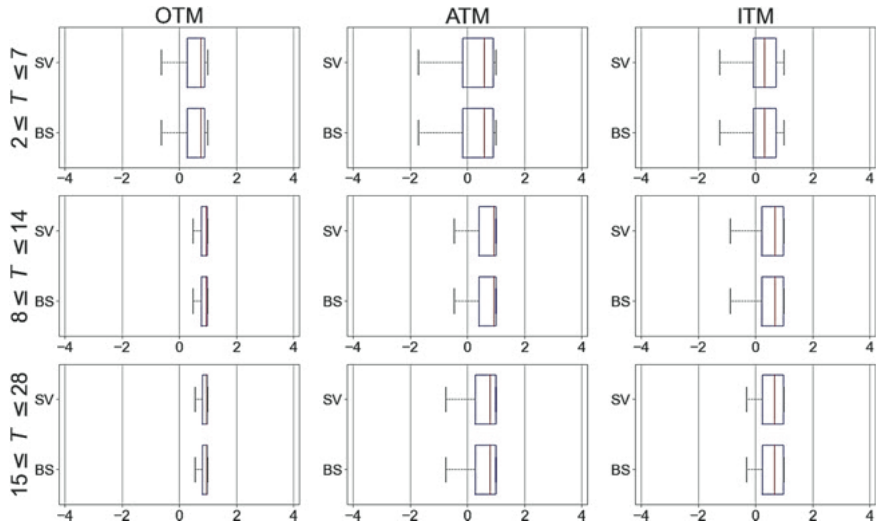


Figure 15: Relative hedging errors for inverse put options using the dynamic delta hedge ■ Deribit_inverse_BTC_options_hedging

2. Dynamic delta-gamma hedging

We need to use another option with a different strike price to attain a delta-gamma-neutral portfolio. Suppose we are hedging in discrete time t for $t = 0, 1, 2, \dots, T$. Let $P_2(t)$, $\Delta_2(t)$, and $\Gamma_2(t)$ be the prices for the delta and gamma of another traded option at time t , respectively. Consider the delta-gamma neutral portfolio, which is composed of the following:

1. A short position of an inverse option, $-P(t)$, denominated in BTC.

2. Long $\left(\Delta(t) - \Delta_2(t) \frac{\Gamma(t)}{\Gamma_2(t)} \right)$ BTCs.

3. Long $\frac{\Gamma(t)}{\Gamma_2(t)}$ the position of another traded inverse option, denominated in BTC.

4. A position in the money market, $B(t)$, denominated in USD.

Let $\Pi(t)$ denote the value of this portfolio in USD. First, set

$$B(0) = P(0) \overline{S(0)} - \left(\Delta(0) - \Delta_2(0) \frac{\Gamma(0)}{\Gamma_2(0)} \right) S(0) - \frac{\Gamma(0)}{\Gamma_2(0)} P_2(0) \overline{S(0)}.$$

Then, we have $\Pi(0) = 0$. Further, we use $\overline{S(0)}$ to denote that it is a constant to be consistently denoted in USD that will not be affected by changes in $S(t)$. For each time with $t \neq T$ we adjust the position of BTC and another traded option and add value changes in long positions to the money market account:

$$B(t) = e^{r(t-(t-1))} \left[\left(\Delta(t) - \Delta_2(t) \frac{\Gamma(t)}{\Gamma_2(t)} \right) - \left(\Delta(t-1) - \Delta_2(t-1) \frac{\Gamma(t-1)}{\Gamma_2(t-1)} \right) \right] S(t) \\ - \left(\frac{\Gamma(t)}{\Gamma_2(t)} - \frac{\Gamma(t-1)}{\Gamma_2(t-1)} \right) P_2(t) S(t)$$

As a result, we have

$$\Pi(t) = -P(t) S(t) + \left(\Delta(t) - \Delta_2(t) \frac{\Gamma(t)}{\Gamma_2(t)} \right) S(t) + \frac{\Gamma(t)}{\Gamma_2(t)} P_2(t) S(t) + B(t).$$

We get the hedging portfolio value $\Pi(T)$ by repeating this procedure until maturity. To measure the performance of the hedge, we determine the discounted relative hedging error,

$$\pi = \frac{e^{-rT} \Pi(T)}{P(0) \bar{S}(0)}$$

Since another traded option is involved when implementing a delta-gamma hedge, we empirically chose the one with the same type and time-to-maturity issued on the same date but with a different and closest strike available. To present the results, we divide the contracts into three groups based on their time-to-maturities: $2 \leq T \leq 7$, $8 \leq T \leq 14$, and $15 \leq T \leq 28$. Figure 16 shows the hedging performance on inverse call options using dynamic delta-gamma hedging for each moneyness-maturity category.

The SV model performs better for the OTM and ITM contracts with $T \geq 8$, while the other categories are similar between the two models. As for the put options shown in 17, the SV model performs better for the OTM contracts and ATM contracts with $T \geq 8$. The ITM contracts in all categories are similar. In addition, all the box plots in the delta-gamma hedge have their center close to zero in contrast to the dynamic delta hedge.

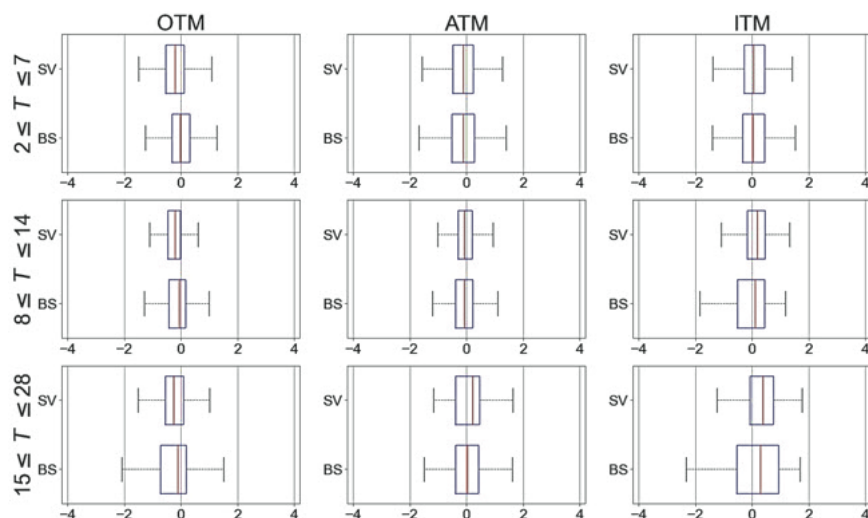


Figure 16: Relative hedging errors for inverse call options using dynamic delta-gamma hedge  Deribit_inverse_BTC_options_hedging

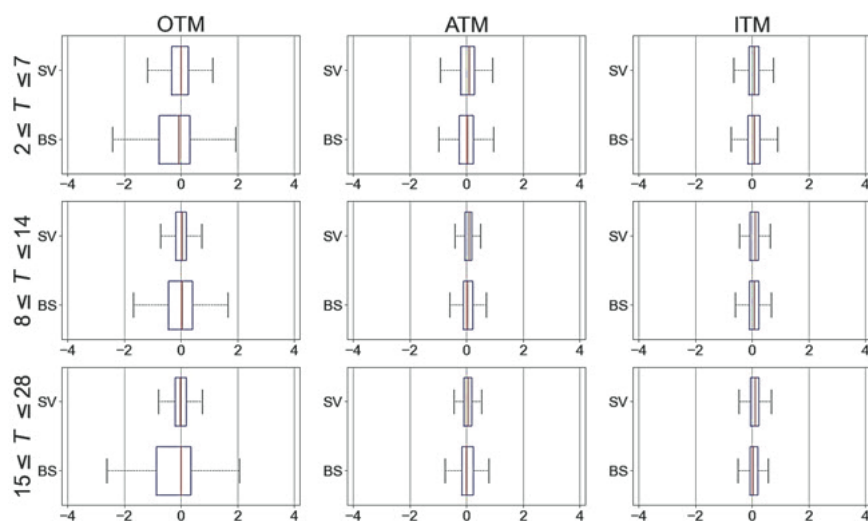


Figure 17: Relative hedging errors for inverse put options using dynamic delta-gamma hedge  Deribit_inverse_BTC_options_hedging

3. Dynamic delta-vega hedging

Like delta-gamma hedging, we need another traded option with a different strike price to construct a delta-vega-neutral portfolio. Suppose we are hedging in discrete time t for $t = 0, 1, 2, \dots, T$. Let $P_2(t)$, $\Delta_2(t)$, and $\mathcal{V}_2(t)$ be the prices of the delta and vega of another traded option at time t , respectively. Consider the delta-vega neutral portfolio, which is composed of the following:

1. A short position of an inverse option, $-P(t)$, denominated in BTC.
2. Long $\Delta(t) - \Delta_2(t) \frac{\mathcal{V}(t)}{\mathcal{V}_2(t)}$ BTCs.
3. Long $\frac{\mathcal{V}(t)}{\mathcal{V}_2(t)}$ the position of another traded inverse option, denominated in BTC.
4. A position in the money market, $B(t)$, denominated in USD.

Let $\Pi(t)$ denote the value of this delta-neutral portfolio in USD. First, set

$$B(0) = P(0) \overline{S(0)} - \left(\Delta(0) - \Delta_2(0) \frac{\mathcal{V}(0)}{\mathcal{V}_2(0)} \right) S(0) - \frac{\mathcal{V}(0)}{\mathcal{V}_2(0)} P_2(0) \overline{S(0)}.$$

Then, we have $\Pi(0) = 0$. Further, we use $\overline{S(0)}$ to denote that it is a constant to be consistently denoted in USD that will not be affected by changes in $S(t)$. For each time with $t \neq T$ we adjust the position of BTC and another traded option and add value changes in long positions to the money market account:

$$B(t) = e^{r(t-(t-1))} \left[\left(\Delta(t) - \Delta_2(t) \frac{\mathcal{V}(t)}{\mathcal{V}_2(t)} \right) - \left(\Delta(t-1) - \Delta_2(t-1) \frac{\mathcal{V}(t-1)}{\mathcal{V}_2(t-1)} \right) \right] S(t) \\ - \left(\frac{\mathcal{V}(t)}{\mathcal{V}_2(t)} - \frac{\mathcal{V}(t-1)}{\mathcal{V}_2(t-1)} \right) P_2(t) S(t)$$

As a result, we have the following:

$$\Pi(t) = -P(t) S(t) + \left(\Delta(t) - \Delta_2(t) \frac{\mathcal{V}(t)}{\mathcal{V}_2(t)} \right) S(t) + \frac{\mathcal{V}(t)}{\mathcal{V}_2(t)} P_2(t) S(t) + B(t).$$

We get the hedging portfolio value $\Pi(T)$ by repeating this procedure until maturity. To measure the performance of hedging, we determine the discounted relative hedging error,

$$\pi = \frac{e^{-rT} \Pi(T)}{P(0) \bar{S}(0)}$$

Similar to dynamic delta-gamma hedging, another traded option is involved. We empirically chose the one with the same type and time-to-maturity issued on the same date but with a different and closest strike available. To present the results, we divide the contracts into three groups based on their time-to-maturities: $2 \leq T \leq 7$, $8 \leq T \leq 14$, and $15 \leq T \leq 28$. Figure 18 shows the hedging performance on inverse call options using the dynamic delta-vega hedge for each moneyness-maturity category. It shows that under the SV model, the ATM and ITM contracts have more minor variances in comparison to the BS model, while the OTM contracts are similar. Figure 19 shows the hedging performances for the case of put options and are the total opposite of the results in the case of call options. OTM contracts perform better under the SV model, while ATM and ITM contracts perform better under the BS model. Finally, the medians in boxplots are mostly close to zero.

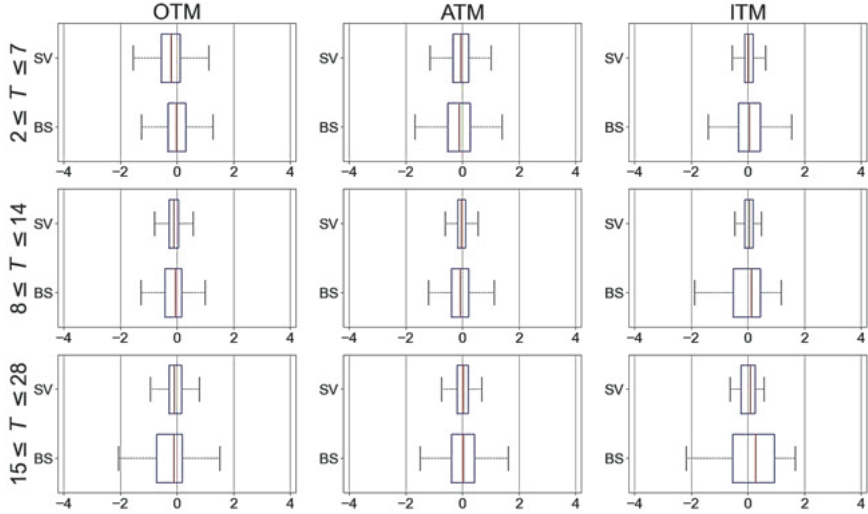


Figure 18: Relative hedging errors for inverse call options using dynamic delta-vega hedge  Deribit_inverse_BTC_options_hedging

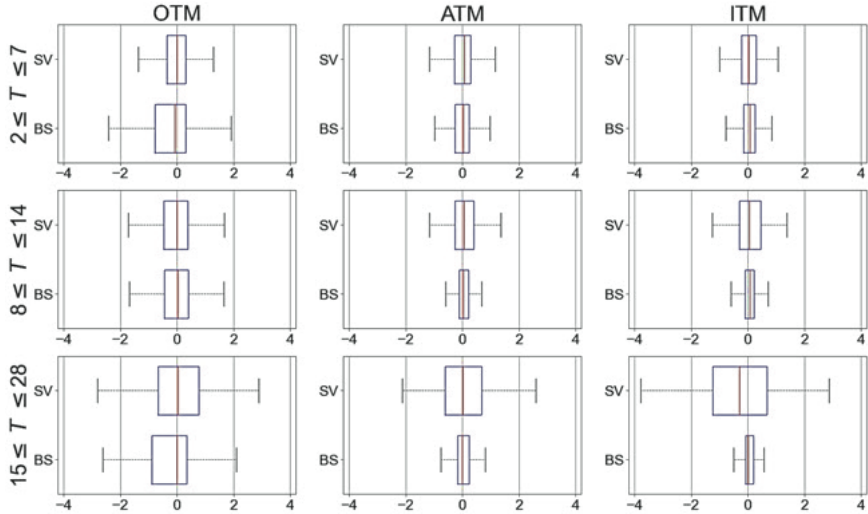


Figure 19: Relative hedging errors for inverse put options using dynamic delta-vega hedge  Deribit_inverse_BTC_options_hedging

For a robustness check, we include more data from April 1 to June 29, 2022, in our analysis. For brevity, we omit to paste similar empirical results. But, we remark that the SV model outperforms the BS model in in-sample and out-of-sample pricing in the new time frame. For dynamic hedging, the BS and SV are indistinguishable. But, for dynamic delta-gamma hedging and dynamic delta-vega hedging, the SV model outperforms the BS model because it produces relative hedging errors of a narrower range. All our codes are available in quantlet.com.

V. Conclusion

In this paper, we derive novel Greek formulae for the BTC-denominated Deribit BTC options under the BS model and Heston stochastic volatility model to compare dynamic hedging with actual data from the crypto market. The results show that the SV model outperforms the BS model in in-sample and out-of-sample pricing. Furthermore, we evaluate the dynamic delta, delta-gamma, and delta-vega hedging. Our analysis shows these two models are indistinguishable in dynamic delta hedging. In dynamic delta-gamma hedging, the SV model performs better on the OTM and ATM inverse put options, particularly for time-to-maturity greater than a week. Lastly, in dynamic delta-vega hedge, the SV model significantly outperforms the BS model for call options but performs worse for put options. In conclusion, adding the SV feature improves the hedging performance of BTC-denominated Deribit BTC options.

For future research, BTC-denominated Deribit BTC options with longer maturity should be considered because our empirical analysis is limited to BTC-denominated Deribit BTC options with a maturity of fewer than 28 days. Second, advanced models, such as stochastic volatility with jumps, should be implemented for BTC-denominated Deribit BTC options. Third, it is interesting to develop variance reduction for calibrating implied parameters under complex dynamics. Further applications based on BTC-denominated Deribit BTC options' empirical behavior are worth deeper exploration.

A. Appendices

Initially, we briefly cover some preliminaries for the following proofs. According to our simulation scheme, the payoff function can be rewritten as

$$\begin{aligned}\varphi^i &= S_T^{-1} \max(\omega(S_T - K), 0) = \omega \left(1 - \frac{K}{S_T} \right) I_{\{\omega(S_T - K) > 0\}} \\ &= \omega \left(1 - \frac{K}{S_0 g(Z_X, Z_Y)} \right) I_{\{\omega(S_T - K) > 0\}}\end{aligned}$$

where $S_T = S_0 g(Z_X, Z_Y)$ and $g(Z_X, Z_Y)$ refers to the randomness that is independent of S_0 .

To derive the parameter derivative $D_{\theta\varphi}(\theta, x)$, a key step is to transform the valid domain of the condition $\omega(S_T - K) > 0$ into equivalent support, which can be represented as $x_k > \chi(\theta, x_{-k})$ with suitable x_k and function χ . Here, based on our simulation scheme, we aim to derive χ by concentrating on the domain of $Z_{X,T}$. In other words, let Ω denote the range of (Z_X, Z_Y) , then the desired support for call options should satisfy

$$\{(Z_X, Z_Y) \in \Omega : S_T > K\} = \{(Z_X, Z_Y) \in \Omega : Z_{X,T} > \chi(S_0, V_0, Z_{X,-T}, Z_Y)\}$$

Likewise, in the case of put options, it should meet

$$\{(Z_X, Z_Y) \in \Omega : S_T < K\} = \{(Z_X, Z_Y) \in \Omega : Z_{X,T} < \chi(S_0, V_0, Z_{X,-T}, Z_Y)\}$$

By solving $S_T = K$, we get

$$\begin{aligned}\chi &:= \chi(S_0, V_0, Z_{X,-T}, Z_Y) \\ &= \frac{1}{\sqrt{1-\rho^2}} \left[\frac{\log \left(\frac{K}{S_0 h(Z_{X,-T}, Z_Y)} \right) - \left(r - \frac{V_T}{2} \right)}{\sqrt{V_T}} - \rho \cdot Z_{Y,T} \right]\end{aligned}$$

To conserve space, we have summarized the main results here. For further derivation details, please refer to Lyuu et al. (2019) and Chang (2022). In the following sections of proofs, we mainly consider χ and $I_{\{\omega(S_T-K)>0\}}$ as functions of a parameter of interest θ and Z_X .

1. Proof of Theorem 1

The parameter derivative of $\wp(S_0, Z_X, Z_Y)$ with respect to S_0 is:

$$\begin{aligned}D_{S_0} \wp(S_0, Z_X, Z_Y) &= \omega \left(\frac{1}{S_0^2} \frac{K}{g(Z_X, Z_Y)} \right) I_{\{\omega(S_T-K)>0\}} \\ &\quad + \omega \left(1 - \frac{1}{S_0} \frac{K}{g(Z_X, Z_Y)} \right) (-\omega) \delta_{\chi(S_0, Z_{X,-T}, Z_Y)}^T \frac{\partial \chi(S_0, Z_{X,-T}, Z_Y)}{\partial S_0} \\ &= \omega \left(\frac{1}{S_0^2} \frac{K}{g(Z_X, Z_Y)} \right) I_{\{\omega(S_T-K)>0\}} \\ &\quad - \left(1 - \frac{1}{S_0} \frac{K}{g(Z_X, Z_Y)} \right) \delta_{\chi(S_0, Z_{X,-T}, Z_Y)}^T \frac{\partial \chi(S_0, Z_{X,-T}, Z_Y)}{\partial S_0}\end{aligned}$$

With $Z_X, Z_Y \sim \mathcal{N}_T(0, \mathbb{I}_T)$ under the expectation, then the integral for the latter part equals:

$$\begin{aligned}
 & \int_{\mathbb{R}^T} \int_{\mathbb{R}^T} \left(1 - \frac{1}{S_0} \frac{K}{g(Z_X, Z_Y)}\right) \delta_{\chi(S_0, Z_{X,-T}, Z_Y)}^T \frac{\partial \chi(S_0, Z_{X,-T}, Z_Y)}{\partial S_0} f_{Z_Y}(y) f_{Z_X}(x) dy dx \\
 &= \int_{\mathbb{R}^{T-1}} \int_{\mathbb{R}^T} \left(1 - \frac{1}{S_0} \frac{K}{K/S_0}\right) \frac{\partial \chi(S_0, Z_{X,-T}, Z_Y)}{\partial S_0} f_{Z_Y}(y) f_{Z_X}(\tilde{x}) dy dx_{-T} \\
 &= \int_{\mathbb{R}^{T-1}} \int_{\mathbb{R}^T} (1 - 1) \frac{\partial \chi(S_0, Z_{X,-T}, Z_Y)}{\partial S_0} f_{Z_Y}(y) f_{Z_X}(\tilde{x}) dy dx_{-T} = 0
 \end{aligned}$$

where $\tilde{x} = (x_1, x_2, \dots, x_{T-1}, \chi)$. Hence, the delta formula remains:

$$\begin{aligned}
 \Delta &= e^{-rT} \mathbb{E} \left[\frac{\partial \wp}{\partial S_0} \right] = \mathbb{E} [D_{S_0} \wp(S_0, Z_X, Z_Y)] \\
 &= \mathbb{E} \left[\omega \left(\frac{1}{S_0^2} \frac{K}{g(Z_X, Z_Y)} \right) I_{\{\omega(S_T - K) > 0\}} \right] \\
 &= \mathbb{E} \left[\omega \left(\frac{1}{S_0} \frac{K}{S_T} \right) I_{\{\omega(S_T - K) > 0\}} \right].
 \end{aligned}$$

2. Proof of Theorem 2

Consider the payoff function based on the formula of Δ :

$$\wp_d = \omega \left(\frac{1}{S_0^2} \frac{K}{g(Z_X, Z_Y)} \right) I_{\{\omega(S_T - K) > 0\}}$$

The parameter derivative $\varphi_d(S_0, Z_X, Z_Y)$ w.r.t S_0 is:

$$\begin{aligned}
 D_{S_0} \varphi_d(S_0, Z_X, Z_Y) &= \omega \left(\frac{-2}{S_0^3} \frac{K}{g(Z_X, Z_Y)} \right) I_{\{\omega(S_T - K) > 0\}} \\
 &+ \omega \left(\frac{1}{S_0^2} \frac{K}{g(Z_X, Z_Y)} \right) (-\omega) \delta_{\chi(S_0, V_0, Z_{X,-T}, Z_Y)}^k \frac{\partial \chi(S_0, V_0, Z_{X,-T}, Z_Y)}{\partial S_0} \\
 &= \omega \left(\frac{-2}{S_0^3} \frac{K}{g(Z_X, Z_Y)} \right) I_{\{\omega(S_T - K) > 0\}} \\
 &- \left(\frac{1}{S_0^2} \frac{K}{g(Z_X, Z_Y)} \right) \delta_{\chi(S_0, V_0, Z_{X,-T}, Z_Y)}^k \frac{\partial \chi(S_0, V_0, Z_{X,-T}, Z_Y)}{\partial S_0}
 \end{aligned}$$

With $Z_X, Z_Y \sim \mathcal{N}_T(0, \mathbb{I}_T)$ under the expectation, then the integral for the latter part equals:

$$\begin{aligned}
 &\int_{\mathbb{R}^T} \int_{\mathbb{R}^T} \left(\frac{1}{S_0^2} \frac{K}{g(Z_X, Z_Y)} \right) \delta_{\chi(S_0, V_0, Z_{X,-T}, Z_Y)}^T \frac{\partial \chi(S_0, V_0, Z_{X,-T}, Z_Y)}{\partial S_0} f_{Z_Y}(y) f_{Z_X}(x) dy dx \\
 &= \int_{\mathbb{R}^{T-1}} \int_{\mathbb{R}^T} \left(\frac{1}{S_0^2} \frac{K}{S_0} \right) \frac{\partial \chi(S_0, V_0, Z_{X,-T}, Z_Y)}{\partial S_0} f_{Z_Y}(y) f_{Z_X}(\tilde{x}) dy dx_{-T} \\
 &= \int_{\mathbb{R}^{T-1}} \int_{\mathbb{R}^T} \frac{1}{S_0} \frac{\partial \chi(S_0, V_0, Z_{X,-T}, Z_Y)}{\partial S_0} f_{Z_Y}(y) \frac{f_{Z_X}(\tilde{x})}{f_{Z_X,-T}(x)} f_{Z_X,-T}(x) dy dx_{-T} \\
 &= \int_{\mathbb{R}^{T-1}} \int_{\mathbb{R}^T} \frac{1}{S_0} \frac{\partial \chi(S_0, V_0, Z_{X,-T}, Z_Y)}{\partial S_0} f_{Z_Y}(y) f_{Z_X,T}(\chi) f_{Z_X,-T}(x) dy dx_{-T} \\
 &= \mathbb{E}^* \left[\frac{1}{S_0} f_{Z_X,T}(\chi) \frac{\partial \chi(S_0, V_0, Z_{X,-T}, Z_Y)}{\partial S_0} \right]
 \end{aligned}$$

where $Z_{X,-T} \sim \mathcal{N}(0, \mathbb{I}_{T-1})$, and $Z_Y \sim \mathcal{N}(0, \mathbb{I}_T)$ under $\mathbb{E}^*[\cdot]$. Hence, the formula for Γ is:

$$\begin{aligned} \Gamma &= e^{-rT} \mathbb{E} \left[\frac{\partial^2 \wp}{\partial S_0^2} \right] = \mathbb{E} [D_{S_0} \wp_d(S_0, Z_X, Z_Y)] \\ &= \mathbb{E} \left[\omega \left(\frac{-2}{S_0^3} \frac{K}{g(\chi)} \right) I_{\{\omega(S_T - K) > 0\}} \right] - \mathbb{E}^* \left[\frac{1}{S_0} f_{Z_X, T}(\chi) \frac{\partial \chi(S_0, V_0, Z_{X,-T}, Z_Y)}{\partial S_0} \right] \\ &= \mathbb{E} \left[\omega \left(\frac{-2}{S_0^2} \frac{K}{S_T} \right) I_{\{\omega(S_T - K) > 0\}} \right] - \mathbb{E}^* \left[\frac{1}{S_0} f_{Z_X, T}(\chi) \frac{\partial \chi(S_0, V_0, Z_{X,-T}, Z_Y)}{\partial S_0} \right] \end{aligned}$$

3. Proof of Theorem 3

Let $v_0 = \sqrt{V_0}$. The parameter derivative $\wp(V_0, Z_X, Z_Y)$ with respect to v_0 is:

$$\begin{aligned} D_{v_0} \wp(V_0, Z_X, Z_Y) &= \omega \left(\frac{K}{S_0} \cdot \frac{1}{g(V_0, Z_X, Z_Y)^2} \frac{\partial g(V_0, Z_X, Z_Y)}{\partial V_0} \frac{\partial V_0}{\partial v_0} \right) I_{\{\omega(S_T - K) > 0\}} \\ &\quad + \omega \left(1 - \frac{1}{S_0} \frac{K}{g(V_0, Z_X, Z_Y)} \right) (-\omega) \delta_{\chi(V_0, Z_{X,-T}, Z_Y)}^T \frac{\partial \chi(V_0, Z_{X,-T}, Z_Y)}{\partial V_0} \end{aligned}$$

Similarly, the integral for the latter part equals 0. Next, to find the explicit form of $\frac{\partial g(V_0, Z_X, Z_Y)}{\partial V_0}$, note $g(V_0, Z_X, Z_Y) = \prod_{t=1}^T e^{\gamma_t}$. Then by the chain rule,

$$\begin{aligned}
\frac{\partial g(V_0, Z_X, Z_Y)}{\partial V_0} &= \sum_{j=1}^T \left[\left(\prod_{\substack{t=1 \\ t \neq j}}^T e^{\gamma_t} \right) \frac{\partial e^{\gamma_j}}{\partial V_0} \right] \\
&= \sum_{j=1}^T \left[\left(\prod_{\substack{t=1 \\ t \neq j}}^T e^{\gamma_t} \right) e^{\gamma_j} \frac{\partial \gamma_j}{\partial V_0} \right] = \left(\prod_{t=1}^T e^{\gamma_t} \right) \sum_{j=1}^T \frac{\partial \gamma_j}{\partial V_0}
\end{aligned}$$

To take this further, we derive the explicit form of the intermediate term $\frac{\partial \gamma_j}{\partial V_0}$.

Note $V_t = \alpha + \beta V_{t-1} + \sigma_v \sqrt{V_{t-1}} Y_t$. Then

$$\frac{\partial V_t}{\partial V_{t-1}} = \beta + \frac{\sigma_v Y_t}{2\sqrt{V_{t-1}}} \stackrel{\text{def}}{=} G(V_{t-1}, Y_t)$$

1. Consider $\gamma_1 = \left(r - \frac{V_1}{2} \right) + \sqrt{V_1} X_1$, then $\frac{\partial \gamma_1}{\partial V_0} = \left(-\frac{1}{2} + \frac{X_1}{2\sqrt{V_1}} \right) \frac{\partial V_1}{\partial V_0}$
2. Consider $\gamma_2 = \left(r - \frac{V_2}{2} \right) + \sqrt{V_2} X_2$, then $\frac{\partial \gamma_2}{\partial V_0} = \left(-\frac{1}{2} + \frac{X_2}{2\sqrt{V_2}} \right) \frac{\partial V_2}{\partial V_1} \frac{\partial V_1}{\partial V_0}$
3. It can be concluded by induction that for $j = 1, \dots, T$,

$$\frac{\partial \gamma_j}{\partial V_0} = \left(-\frac{1}{2} + \frac{X_j}{2\sqrt{V_j}} \right) \left(\prod_{t=1}^j \frac{\partial V_t}{\partial V_{t-1}} \right) = \left(-\frac{1}{2} + \frac{X_j}{2\sqrt{V_j}} \right) \left(\prod_{t=1}^j G(V_{t-1}, Y_t) \right)$$

Consequently, we can get:

$$\begin{aligned} \frac{\partial g(V_0, Z_X, Z_Y)}{\partial V_0} &= \left(\prod_{t=1}^T e^{\gamma_t} \right) \sum_{j=1}^T \frac{\partial \gamma_j}{\partial V_0} = g(V_0, Z_X, Z_Y) \sum_{j=1}^T \frac{\partial \gamma_j}{\partial V_0} \\ &= g(V_0, Z_X, Z_Y) \sum_{j=1}^T \left[\left(-\frac{1}{2} + \frac{X_j}{2\sqrt{V_j}} \right) \left(\prod_{t=1}^j G(V_{t-1}, Y_t) \right) \right] \end{aligned}$$

Hence, the formula for vega is:

$$\begin{aligned} \mathcal{V} &= e^{-rT} \mathbb{E} \left[\frac{\partial \wp}{\partial v_0} \right] = \mathbb{E} [D_{v_0} \wp(V_0, Z_X, Z_Y)] \\ &= \mathbb{E} \left[\omega \left(\frac{K}{S_0} \cdot \frac{1}{g(V_0, Z_X, Z_Y)^2} \frac{\partial g(V_0, Z_X, Z_Y)}{\partial V_0} \frac{\partial V_0}{\partial v_0} \right) I_{\{\omega(S_T - K) > 0\}} \right] \\ &= \mathbb{E} \left[\omega \left(\frac{K}{S_T} \sum_{j=1}^T \left[\left(-\frac{1}{2} + \frac{X_j}{2\sqrt{V_j}} \right) \left(\prod_{t=1}^j G(V_{t-1}, Y_t) \right) \right] 2\sqrt{V_0} \right) I_{\{\omega(S_T - K) > 0\}} \right] \\ &= \mathbb{E} \left[\omega \left(\frac{K}{S_T} \sqrt{V_0} \sum_{j=1}^T \left[\left(-1 + \frac{X_j}{\sqrt{V_j}} \right) \left(\prod_{t=1}^j G(V_{t-1}, Y_t) \right) \right] \right) I_{\{\omega(S_T - K) > 0\}} \right] \end{aligned}$$

References

- Alexander, C., D. Chen, and A. Imeraj (2022). Crypto quanto and inverse options in a black-scholes world. Available at SSRN <https://ssrn.com/abstract=3893037>.
- Alexander, C. and A. Imeraj (2021). Inverse options in a Black-Scholes world. Available at arXiv: <https://arxiv.org/abs/2107.12041>.
- Bakshi, G., C. Cao, and Z. Chen (1997). Empirical performance of alternative option pricing models. *The Journal of Finance* 52(5), 2003-2049.
- Baur, D. G., K. Hong, and A. D. Lee (2018). Bitcoin: Medium of exchange or speculative assets? *Journal of International Financial Markets, Institutions and Money* 54, 177-189.
- Broadie, M. and P. Glasserman (1996). Estimating security price derivatives using simulation. *Management Science* 42(2), 269-285.
- Cao, M. and B. Celik (2021). Valuation of bitcoin options. *Journal of Futures Markets* 41(7), 1007-1026.
- Cao, X.-R. (1985). Convergence of parameter sensitivity estimates in a stochastic experiment. *IEEE Transactions on Automatic Control* 30(9), 845-853.
- Chang, Y.-C. (2022). Pricing and hedging inverse BTC options with Heston's stochastic volatility model. Master's thesis, National Yang Ming Chiao Tung University.
- Cui, Y., S. del Bano Rollin, and G. Germano (2017). Full and fast calibration of the Heston stochastic volatility model. *European Journal of Operational Research* 263(2), 625-638.
- Davis, M. H. and M. P. Johansson (2006). Malliavin Monte Carlo greeks for jump diffusions. *Stochastic Processes and their Applications* 116(1), 101-129.
- Fengler, M. R. (2006). *Semiparametric modeling of implied volatility*. Springer

Science & Business Media.

- Franke, J., W. K. Härdle, and C. M. Hafner (2004). *Statistics of financial markets*, Volume 2. Berlin: Springer.
- Glasserman, P. (2004). *Monte Carlo methods in financial engineering*. New York: Springer.
- Heidergott, B. and H. Leahu (2010). Weak differentiability of product measures. *Mathematics of Operations Research* 35(1), 27-51.
- Heston, S. L. (1993). A closed-form solution for options with stochastic volatility with applications to bond and currency options. *The Review of Financial Studies* 6(2), 327-343.
- Hou, A.-J., W. Wang, C. Y. Chen, and W. K. Härdle (2020). Pricing cryptocurrency options. *Journal of Financial Econometrics* 18(2), 250-279.
- Jalan, A., R. Matkovskyy, and S. Aziz (2021). The Bitcoin options market: A first look at pricing and risk. *Applied Economics* 53(17), 2026-2041.
- Kawai, R. and A. Takeuchi (2011). Greeks formulas for an asset price model with gamma processes. *Mathematical Finance: An International Journal of Mathematics, Statistics and Financial Economics* 21(4), 723-742.
- Lyu, Y.-D. and H.-W. Teng (2011). Unbiased and efficient Greeks of financial options. *Finance and Stochastics* 15(1), 141-181.
- Lyu, Y.-D., H.-W. Teng, Y.-T. Tseng, and S.-X. Wang (2019). A systematic and efficient simulation scheme for the Greeks of financial derivatives. *Quantitative Finance* 19(7), 1199-1219.
- Madan, D. B., S. Reyners, and W. Schoutens (2019). Advanced model calibration on bitcoin options. *Digital Finance* 1(1), 117-137.
- Matic, J. L., P. N. Packham, and W. K. Härdle (2021). Hedging cryptocurrency options. Available at arXiv: <https://arxiv.org/abs/2112.06807>.
- Mrázek, M., J. Pospíšil, and T. Sobotka (2016). On calibration of stochastic and fractional stochastic volatility models. *European Journal of Operational*

- Research* 254(3), 1036-1046.
- Pagnottoni, P. and T. Dimpfl (2019). Price discovery on Bitcoin markets. *Digital Finance* 1(1), 139-161.
- Satoshi, N. (2008). Bitcoin: A peer-to-peer electronic cash system. *Decentralized Business Review*, 21260.
- Teng, H.-W. and W. K. Härdle (2022). Financial analytics of inverse BTC options in a stochastic volatility world. Available at SSRN: <http://ssrn.com/abstract=4238213>.
- Thoma, P. (2012). *Efficient calculation of the Greeks: An application of measure valued differentiation*. Ph. D. thesis, Universität Wien.
- Zhu, J. (2009). *Applications of Fourier transform to smile modeling: Theory and implementation*. Springer Berlin, Heidelberg.
- Zulfqar, N. and S. Gulzar (2021). Implied volatility estimation of bitcoin options and the stylized facts of option pricing. *Financial Innovation* 7(1), 1-30.